Multiple Types of Topological Fermions in Transition Metal Silicides

Peizhe Tang,[1] Quan Zhou,[1] and Shou-Cheng Zhang[1,2]

[1]*Department of Physics, McCullough Building, Stanford University, Stanford, California 94305-4045, USA*
[2]*Stanford Institute for Materials and Energy Sciences, SLAC National Accelerator Laboratory, Menlo Park, California 94025, USA*

Exotic massless fermionic excitations with nonzero Berry flux, other than the Dirac and Weyl fermions, could exist in condensed matter systems under the protection of crystalline symmetries, such as spin-1 excitations with threefold degeneracy and spin-3/2 Rarita-Schwinger-Weyl fermions. Herein, by using the *ab initio* density functional theory, we show that these unconventional quasiparticles coexist with type-I and type-II Weyl fermions in a family of transition metal silicides, including CoSi, RhSi, RhGe, and CoGe, when spin-orbit coupling is considered. Their nontrivial topology results in a series of extensive Fermi arcs connecting projections of these bulk excitations on the side surface, which is confirmed by (001) surface electronic spectra of CoSi. In addition, these stable arc states exist within a wide energy window around the Fermi level, which makes them readily accessible in angle-resolved photoemission spectroscopy measurements.

Introduction.—Three types of fermions play fundamental roles in our understanding of nature: Majorana, Dirac, and Weyl [1]. Much attention has been paid to looking for these fundamental particles in high-energy physics during the past few decades, whereas only a signature of Dirac fermions is captured. Interestingly, the same movement comes up in the field of condensed matter physics [2], and great achievements have been made in the past few years. For example, Majorana-like excitations are detected in superconducting heterostructures [3–6]; Dirac [7–12] and Weyl [13–31] fermions are observed in some compounds. These quasiparticles in solid states not only are important for basic science but also show great potential for practical applications on new devices [32,33].

Because symmetries in condensed matter physics are usually much lower than the Poincaré symmetry in high-energy physics, quasiparticles in solid states are less constrained such that various new types of fermionic excitations are predicted to exist in three-dimensional (3D) lattices [34–39]. Among these allowed by space group (SG) symmetries are spin-1 and spin-3/2 massless fermionic excitations, besides the well-known spin-1/2 case, namely, the Weyl fermion. All of these massless quasiparticles can be described by the low-energy Hamiltonian in a unified manner to the linear order of momentum

$$H = \delta \boldsymbol{k} \cdot \boldsymbol{S}, \qquad (1)$$

where $\delta \boldsymbol{k} = \boldsymbol{k} - \boldsymbol{k}_0$ is the momentum deviation from the crossing point $\boldsymbol{k}_0$ and $\boldsymbol{S}$ stands for the matrices for the pseudospin degree of freedom that satisfy $[\boldsymbol{S}_i, \boldsymbol{S}_j] = i\epsilon_{ijk}\boldsymbol{S}_k$. The definite helicity can be assigned to each energy band of H, and it is related to the nonvanishing Chern number for one energy surface enclosing the crossing point. These band crossings behave as monopoles of the Berry flux. For

example, the Weyl fermion takes 2×2 Pauli matrices and holds a twofold degeneracy; its crossing point carries a topological charge ± 1 [see Fig. 1(a)]. As a generalization, the spin-1 excitation takes 3×3 spin matrices and holds a threefold degeneracy [see Fig. 1(b)]; its crossing point
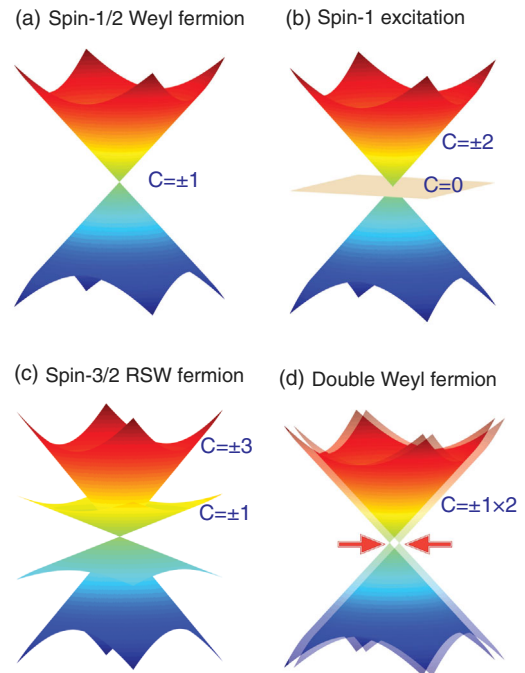
FIG. 1. Energy dispersions for multiple types of topological fermions. (a) The Weyl fermion with $\mathbf{S} = 1/2$. (b) The excitation with $\mathbf{S} = 1$. (c) The Rarita-Schwinger-Weyl fermion with $\mathbf{S} = 3/2$. (d) The double Weyl fermion. The red arrows indicate that two energy crossings should be at the same point for the double Weyl fermion. Chern numbers for upper and lower bands are marked in blue for topological fermions.
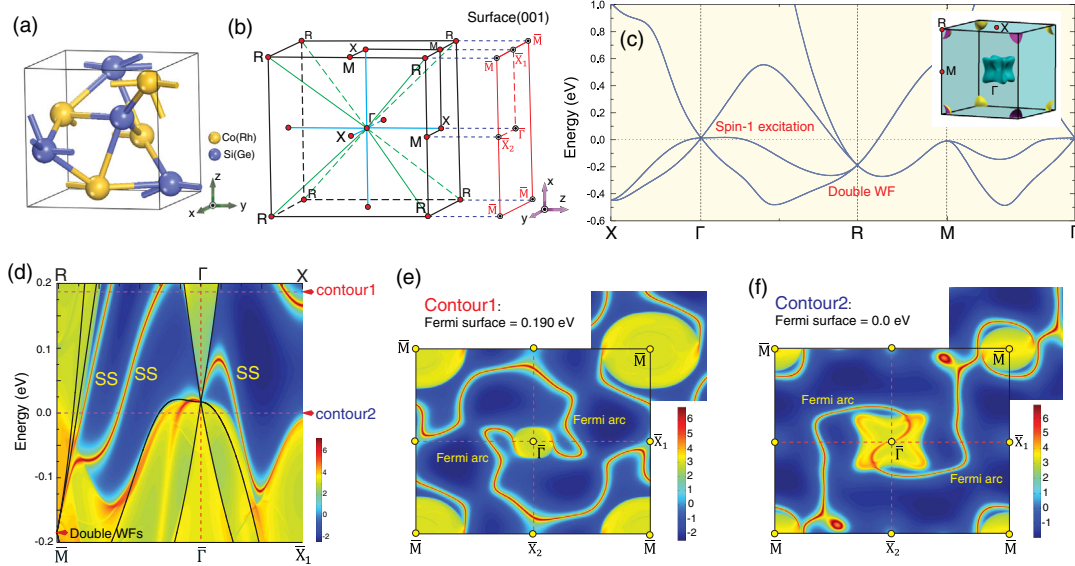
FIG. 2. The crystalline lattice structure, Brillouin zone (BZ), and electronic properties for CoSi without spin-orbit coupling (SOC). (a) The lattice structure and (b) BZ for the CoSi family. The projected BZ of the (001) surface is marked in red lines. (c) The bulk band structure for CoSi along high symmetry lines. The inset is a 3D Fermi surface at the calculated Fermi level. (d) The corresponding electronic spectra for the (001) surface. Bulk bands along lines of R-Γ and Γ-X are plotted in black, in which the lines along R-Γ are rescaled to fit the distance between $\bar{M}$ and $\bar{\Gamma}$ points. (e),(f) The Fermi surface contours on the (001) surface at different energies. The calculated Fermi level is set to be zero.

carries a topological charge ± 2 because of no contribution from the middle band with helicity 0 [34,40]. Spin-3/2 excitations are named as Rarita-Schwinger-Weyl (RSW) fermions [34,41–43], and S takes 4×4 spin matrices. Its Fermi surface has to cross two bands near the crossing point, for example, the helicity 3/2 and 1/2 bands with the topological charges ± 3 and ± 1, respectively [see Fig. 1(c)]. So a spin-3/2 RSW fermion acts as a monopole with topological charge ± 4. Additionally, the time-reversal (TR) symmetry could lead to a nontrivial doubling of these excitations in some situations, which gives birth to double Weyl fermions possessing topological charge ± 2 [see Fig. 1(d)] [44,46,47] and double spin-1 excitations with sixfold degeneracy [34]. On the other hand, besides the massless fermions beyond the Dirac and Weyl models mentioned above, the other kind of new fermions, named as three-component fermions, are predicted and observed in a family of two-element metals AB with WC-type structure [36–39], whose triple degeneracy is protected by the C_{3v} rotation symmetry.

In this Letter, we explore electronic properties for a family of transition metal silicides (CoSi family) based on *ab initio* calculations (see Supplemental Material [48] for computational details). Its bulk states host all of the exotic fermionic quasiparticles mentioned above under different conditions. To our best knowledge, this work is the first attempt to incorporate multiple types of topological fermions in a solid compound that has been synthesized experimentally [56–60]. Around the Fermi level, the conductance in CoSi-family compounds is mainly contributed

by these unconventional excitations with nontrivial topology. Thus, signatures related to quantum anomalies are very likely to be observed in electrical and thermal transport measurements. On the other hand, because these fermionic excitations with different large Chern numbers reside in (or near) either the center or the corner of the Brillouin zone (BZ), the surface states that connect their projections emerge extensively on the side surface, in sharp contrast to most known topological semimetals whose topological charges are ± 1 [13–31] or zero [35–39], and arc states live only within small regions [15,18–25,27–29,36–38,61]. These extensive arc states in CoSi-family compounds offer a great opportunity to fully investigate the nontrivial surface states in experiments.

Lattice structure of the CoSi family.—The family of transition metal silicides includes CoSi [56,57], RhSi [58], CoGe [59], and RhGe [60], which have been synthesized experimentally. All of them have the same cubic lattice with space group $P2_13$ (No. 198) and similar electronic properties. For convenience, we focus on CoSi, a prototype in this family with diamagnetic character [57], in the following discussion. Its lattice structure is shown in Fig. 2(a); each Si site is bonded by four nearest neighboring Co atoms in one unit cell. The corresponding BZ is shown in Fig. 2(b); TR invariant points are plotted by red dots. SG 198 has 12 symmetry operations, which can be generated by three of them: one threefold rotation symmetry along the (111) axis and two twofold screw symmetries along the z and x axis. Therefore, the lattice of CoSi has three twofold and four threefold rotation or screw axes totally.

Electronic structures without SOC.—Figure 2(c) demonstrates the calculated electronic structure and the Fermi surface for CoSi bulk without SOC. Although this compound contains the transition metal, no magnetization is observed in our calculations, and TR symmetry is guaranteed in the whole system, which is consistent with experimental observations [57]. Around the Fermi level, electronic states are contributed only by hole pockets at the Γ point and electron pockets at the R point. For each physical spin, a gapless point with threefold degeneracy is observed above the Fermi level at the center of the BZ, which is stabilized by crystal symmetries (see Supplemental Material [48] for details). Its low-energy physics can be described by spin-1 excitations shown in Fig. 1(b), whose crossing point is a monopole possessing topological charge $+2$. At the R point, we found a band crossing with fourfold degeneracy below the Fermi level, which is a double Weyl fermion with the Chern number -2 [44]. So the total Chern number is zero for the whole Fermi surface in CoSi bulk, which is consistent with no-go theorem [62].

Because of nontrivial topology possessed by hole and electron pockets in the bulk, the Fermi arc surface states can be observed on the side surface. The electronic spectra for the (001) surface is shown in Fig. 2(d). We can see that topological surface states (marked by SS) emerge from projections of spin-1 excitation and a double Weyl fermion at Γ and R points, which are stable in a large energy window. Figures 2(e) and 2(f) demonstrate the Fermi surface contours on the (001) surface at different energies, in which two Fermi arcs connect states at $\bar{\Gamma}$ and $\bar{M}$ points. Especially for the contour at the Fermi level [see Fig. 2(e)], Fermi arcs emerge from the $\bar{\Gamma}$ point directly, which indicates that the middle flat band in spin-1 excitations does not carry a topological charge [see Fig. 1(b)].

Electronic structures with SOC.—Figure 3 shows the bulk band structures for CoSi with SOC. Because of the absence of inversion symmetry in SG 198, the SOC term lifts the degeneracy at an arbitrary non-TR invariant point, except for states on boundaries of the 3D BZ whose double degeneracy is protected by TR and nonsymmorphic screw symmetries [34]. At the center of the BZ, the sixfold degeneracy point is split by SOC into two crossing points with twofold and fourfold degeneracy, respectively. They correspond to a Weyl fermion and a spin-3/2 RSW fermion with topological charge $+4$. And the fourfold degeneracy originates from the TR forced doubling of the underlying two-dimensional irreducible representation of the symmetry group [63]. Meanwhile, a crossing point with sixfold degeneracy is found at the R point. It is realized as a TR doubling of spin-1 excitations protected by nonsymmorphic symmetries [34], and its total topological charge is -4. In stark contrast to three-component fermions [36–39], double Dirac fermions [35], and Weyl fermions [13–31] whose topological charge is ± 1 or zero, the spin-1 and spin-3/2 fermionic excitations carry large Chern numbers; thus, some
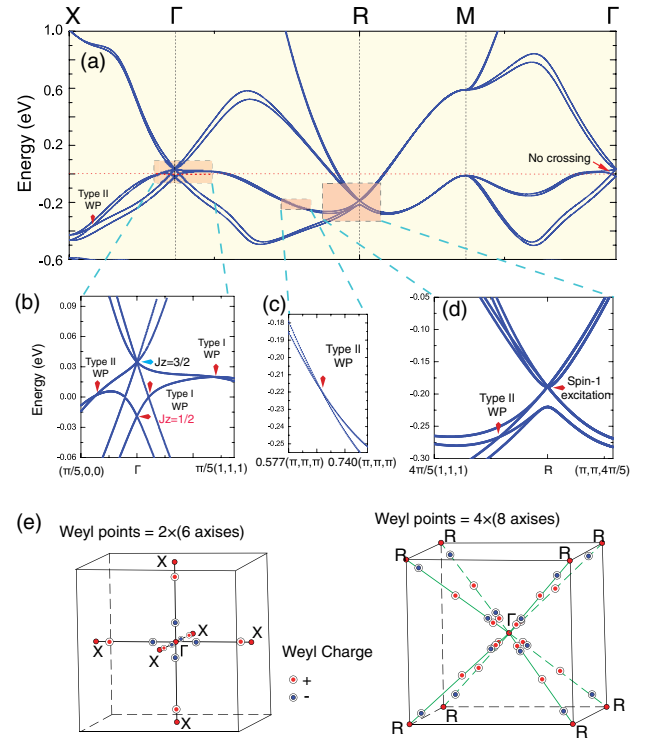
FIG. 3. Electronic structures for CoSi with SOC. (a) The bulk band structure for CoSi along high symmetry lines. (b)–(d) Enlargement of bands in regions marked by red boxes. Weyl fermions are marked by red arrows (including type I and type II). The Rarita-Schwinger-Weyl fermion is marked by a blue arrow. The calculated Fermi level is set to be zero. (e) Schematics of the distribution of Weyl fermions along lines of Γ-X and Γ-R around the Fermi level. The red (blue) dots stand for the Weyl points with a positive (negative) topological charge.

physical phenomena related with topological charges should be observed in this system, such as bulk photogalvanic effect with a large quantized value and multiple Fermi arc surface states. Furthermore, the coexistence of spin-1 and spin-3/2 RSW fermions in a compound with SG 198 is beyond previous studies on unconventional quasiparticles [34].

At the same time, we found CoSi can host type-I and type-II Weyl fermions along symmetry-invariant axes. For bands below the gapless RSW point (see Fig. 3), six pairs of type-II Weyl fermions exist along Γ-X lines; each pair has opposite chiral charges. And four Weyl fermions are observed on each line of Γ-R that is invariant under threefold rotation or screw symmetries. Two of them are type I, and the others are type II. In total, 32 Weyl points exist along these threefold rotation or screw axes [see Fig. 3(e)], and the sum of their topological charges is zero. Similar to previous discussions [45,64], these Weyl fermions in CoSi are generated by the crossing of states with different eigenvalues of rotation or screw symmetries.

In order to demonstrate exotic physics of topological fermions in CoSi with SOC, we explore its electronic spectra on the (001) surface. The calculated results are
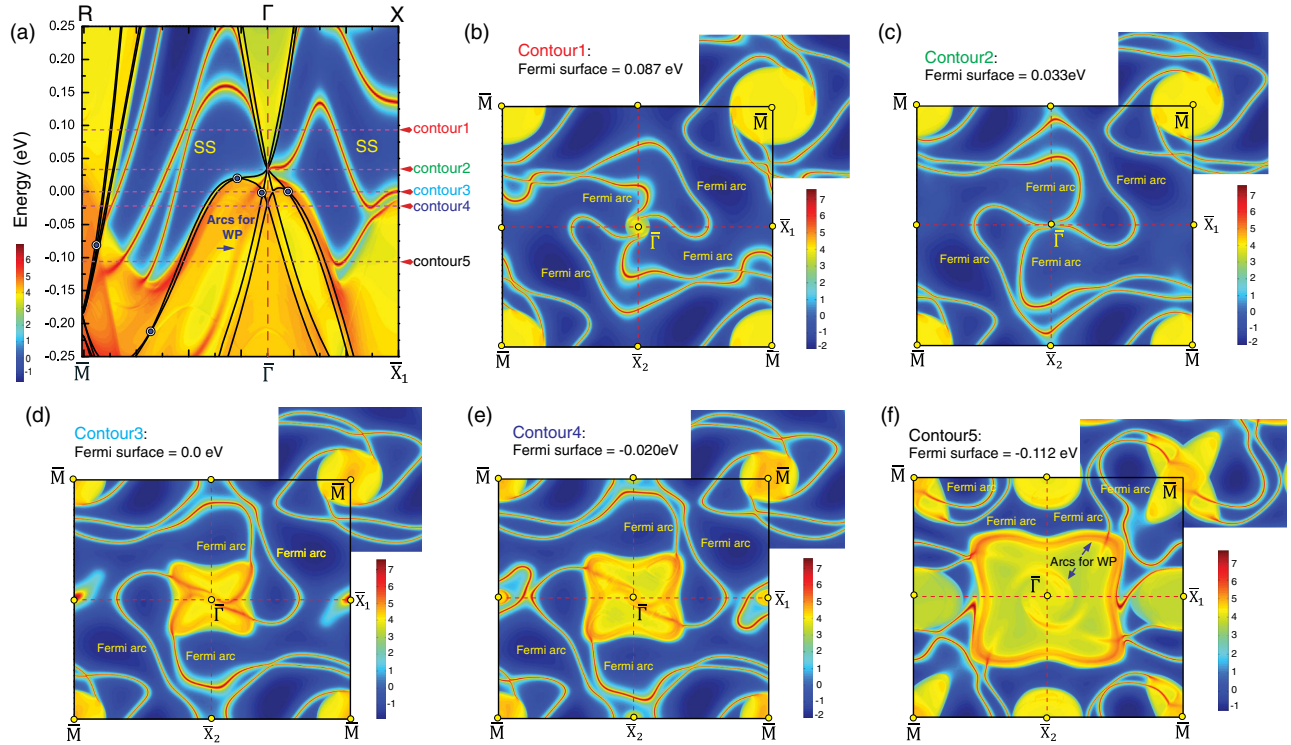
FIG. 4.   The projected electronic spectra for CoSi with SOC. (a) The electronic spectra along high symmetry lines projected to the (001) surface. Bulk bands along lines of R-Γ and Γ-X are plotted as black lines, in which the lines along R-Γ are rescaled to fit the distance between $\bar{M}$ and $\bar{\Gamma}$ points. Type-I and type-II Weyl fermions are marked by blue dots. (b)–(f) The corresponding Fermi surface contours on the (001) surface at different energies. The calculated Fermi level is set to be zero.

shown in Fig. 4. Topologically nontrivial surface states that related to excitations beyond Dirac and Weyl models can be observed clearly on the side surface, which emerge from projections of bulk states at the $\bar{\Gamma}$ point and end at those around the $\bar{M}$ point. In Figs. 4(b)–(f), we show Fermi surface contours at different energies; all of them are above the gapless point with sixfold degeneracy at the R point in the energy scale. In contour 1 [see Fig. 4(b)], states around the $\bar{\Gamma}$ point are projected from bulk conduction bands with helicities of $3/2$ and $1/2$ in the RSW fermion, and their total topological charge is $+4$. So four Fermi arcs are observed around the $\bar{\Gamma}$ point on the (001) surface. When the energy cuts the crossing point in the RSW fermion [see Fig. 4(c)], the arc states emerge from the $\bar{\Gamma}$ point directly, indicating the nontrivial topology carried by the RSW fermion. Furthermore, with a lower energy, projections at the $\bar{\Gamma}$ point are from states with $3/2$ helicity in the RSW fermion below its fourfold gapless point and states in the Weyl fermion at the Γ point. Their total Chern number still is $+4$, and four Fermi arcs are observed in Figs. 4(d)–(f). Similar to cases in TaAs [15,18,20–22] and MoTe$_2$ [23–25,27–29], Fermi arcs contributed by type-I and type-II Weyl fermions in CoSi are coupled with bulk states strongly, although these bulk states still carry nonzero topological charges. Thus, the signature from Weyl fermions is hard to distinguish on the surface spectroscopy.

Herein, we found the possible signal of Fermi arcs contributed by type-II Weyl fermions in Fig. 4(f) and the Lifshitz transition for Fermi arc surface states.

Conclusion.—By using first-principles calculations, we predict that bulk states of CoSi-family compounds host spin-1 excitations, double Weyl fermions, spin-3/2 RSW fermions, and type-I and type-II Weyl fermions in cases without and with SOC. The corresponding extensive Fermi arcs are observed on the (001) surface clearly. Different from previously found topological semimetals, such as the three-component, Dirac, and Weyl fermions, our systems support topological features in a large energy window around the Fermi level and almost on the whole surface BZ. We expect that these electronic signatures can be observed via angle-resolved photoemission spectroscopy on the side surface directly. When a magnetic field is applied to this system to break TR symmetry, these quasiparticles may split to multiple Weyl fermions [34]. Therefore, the anomalous magnetoresistance may be observed via electrical transport measurements, and quantum anomalies may be identified via thermal transports [65]. Because of the large Chern number carried by spin-3/2 and spin-1 excitations, the exotic bulk photogalvanic effects related to chiral charges may be also observed in this system. Therefore, this work not only identifies a series of desired robust topological semimetal candidates but also provides

an ideal platform to explore exotic physical phenomena and future device applications.

Note added.—Recently, we became aware of an e-print aiming at double Weyl points in phonon dispersion for transition metal silicides MSi ($M =$ Fe, Co, Mn, Re, Ru) with SG 198 [66]. After this work was made public through posting as an e-print [67], a similar work, carried out independently by another group, also became public as an e-print [68].

[1] P. B. Pal, Am. J. Phys. **79**, 485 (2011).
[2] N. Armitage, E. Mele, and A. Vishwanath, arXiv:1705.01111 [Rev. Mod. Phys. (to be published)].
[3] M.-X. Wang *et al.*, Science **336**, 52 (2012).
[4] S. Nadj-Perge, I. K. Drozdov, J. Li, H. Chen, S. Jeon, J. Seo, A. H. MacDonald, B. A. Bernevig, and A. Yazdani, Science **346**, 602 (2014).
[5] J. Wang, Q. Zhou, B. Lian, and S.-C. Zhang, Phys. Rev. B **92**, 064520 (2015).
[6] Q. L. He *et al.*, Science **357**, 294 (2017).
[7] Z. Wang, Y. Sun, X.-Q. Chen, C. Franchini, G. Xu, H. Weng, X. Dai, and Z. Fang, Phys. Rev. B **85**, 195320 (2012).
[8] Z. Wang, H. Weng, Q. Wu, X. Dai, and Z. Fang, Phys. Rev. B **88**, 125427 (2013).
[9] P. Tang, Q. Zhou, G. Xu, and S.-C. Zhang, Nat. Phys. **12**, 1100 (2016).
[10] Z. Liu *et al.*, Nat. Mater. **13**, 677 (2014).
[11] Z. Liu *et al.*, Science **343**, 864 (2014).
[12] S.-Y. Xu *et al.*, Science **347**, 294 (2015).
[13] Y. Xu, F. Zhang, and C. Zhang, Phys. Rev. Lett. **115**, 265304 (2015).
[14] H. Weng, C. Fang, Z. Fang, B. A. Bernevig, and X. Dai, Phys. Rev. X **5**, 011029 (2015).
[15] B. Q. Lv, H. M. Weng, B. B. Fu, X. P. Wang, H. Miao, J. Ma, P. Richard, X. C. Huang, L. X. Zhao, G. F. Chen, Z. Fang, X. Dai, T. Qian, and H. Ding, Phys. Rev. X **5**, 031013 (2015).
[16] S.-Y. Xu *et al.*, Science **349**, 613 (2015).
[17] S.-M. Huang *et al.*, Nat. Commun. **6**, 7373 (2015).
[18] Z. Liu *et al.*, Nat. Mater. **15**, 27 (2016).
[19] S.-Y. Xu *et al.*, Nat. Phys. **11**, 748 (2015).
[20] L. Yang *et al.*, Nat. Phys. **11**, 728 (2015).
[21] B. Lv *et al.*, Nat. Phys. **11**, 724 (2015).
[22] Y. Sun, S.-C. Wu, and B. Yan, Phys. Rev. B **92**, 115428 (2015).
[23] A. A. Soluyanov, D. Gresch, Z. Wang, Q. Wu, M. Troyer, X. Dai, and B. A. Bernevig, Nature (London) **527**, 495 (2015).
[24] Y. Sun, S.-C. Wu, M. N. Ali, C. Felser, and B. Yan, Phys. Rev. B **92**, 161107 (2015).
[25] Z. Wang, D. Gresch, A. A. Soluyanov, W. Xie, S. Kushwaha, X. Dai, M. Troyer, R. J. Cava, and B. A. Bernevig, Phys. Rev. Lett. **117**, 056805 (2016).
[26] G. Autès, D. Gresch, M. Troyer, A. A. Soluyanov, and O. V. Yazyev, Phys. Rev. Lett. **117**, 066402 (2016).
[27] K. Deng *et al.*, Nat. Phys. **12**, 1105 (2016).
[28] L. Huang *et al.*, Nat. Mater. **15**, 1155 (2016).
[29] T.-R. Chang *et al.*, Nat. Commun. **7**, 10639 (2016).
[30] K. Koepernik, D. Kasinathan, D. V. Efremov, S. Khim, S. Borisenko, B. Büchner, and J. van den Brink, Phys. Rev. B **93**, 201101 (2016).
[31] G. Chang *et al.*, Sci. Adv. **2**, e1600295 (2016).
[32] Y. Sun, Y. Zhang, C. Felser, and B. Yan, Phys. Rev. Lett. **117**, 146403 (2016).
[33] Y. Wang *et al.*, Nat. Commun. **7**, 13142 (2016).
[34] B. Bradlyn, J. Cano, Z. Wang, M. Vergniory, C. Felser, R. Cava, and B. A. Bernevig, Science **353**, aaf5037 (2016).
[35] B. J. Wieder, Y. Kim, A. M. Rappe, and C. L. Kane, Phys. Rev. Lett. **116**, 186402 (2016).
[36] H. Weng, C. Fang, Z. Fang, and X. Dai, Phys. Rev. B **94**, 165201 (2016).
[37] H. Weng, C. Fang, Z. Fang, and X. Dai, Phys. Rev. B **93**, 241202 (2016).
[38] Z. Zhu, G. W. Winkler, Q. S. Wu, J. Li, and A. A. Soluyanov, Phys. Rev. X **6**, 031003 (2016).
[39] B. Lv *et al.*, Nature (London) **546**, 627 (2017).
[40] J. L. Mañes, Phys. Rev. B **85**, 155118 (2012).
[41] W. Rarita and J. Schwinger, Phys. Rev. **60**, 61 (1941).
[42] L. Liang and Y. Yu, Phys. Rev. B **93**, 045113 (2016).
[43] M. Ezawa, Phys. Rev. B **94**, 195205 (2016).
[44] The double Weyl fermion mentioned in this work is different from the quadratic double-Weyl node [45], although both of them have the Chern number ± 2.
[45] C. Fang, M. J. Gilbert, X. Dai, and B. A. Bernevig, Phys. Rev. Lett. **108**, 266802 (2012).
[46] R. M. Geilhufe, S. S. Borysov, A. Bouhon, and A. V. Balatsky, Sci. Rep. **7**, 7298 (2017).
[47] Y. Xu and L.-M. Duan, Phys. Rev. A **94**, 053619 (2016).
[48] See Supplemental Material at http://link.aps.org/supplemental/10.1103/PhysRevLett.119.206402 for details about the methods of calculations, an effective model of CoSi at the Γ point, and the 3D Fermi surface of CoSi with SOC, which includes [49–55].
[49] P. E. Blöchl, Phys. Rev. B **50**, 17953 (1994).
[50] G. Kresse and D. Joubert, Phys. Rev. B **59**, 1758 (1999).
[51] G. Kresse and J. Furthmüller, Phys. Rev. B **54**, 11169 (1996).
[52] A. A. Mostofi, J. R. Yates, Y.-S. Lee, I. Souza, D. Vanderbilt, and N. Marzari, Comput. Phys. Commun. **178**, 685 (2008).
[53] Q. S. Wu, S. Zhang, H.-F. Song, M. Troyer, and A. A. Soluyanov, arXiv:1703.07789.
[54] S. L. Dudarev, G. A. Botton, S. Y. Savrasov, C. J. Humphreys, and A. P. Sutton, Phys. Rev. B **57**, 1505 (1998).
[55] M. Aroyo, J. Perez-Mato, D. Orobengoa, E. Tasci, G. De La Flor, and A. Kirov, Bulg Chem Commun **43**, 183 (2011).
[56] D. Shinoda, Phys. Status Solidi (a) **11**, 129 (1972).
[57] V. Narozhnyi and V. Krasnorussky, J. Exp. Theor. Phys. **116**, 780 (2013).
[58] S. Geller and E. Wood, Acta Crystallogr. **7**, 441 (1954).

[59] H. Takizawa, T. Sato, T. Endo, and M. Shimada, J. Solid State Chem. **73**, 40 (1988).

[60] V. Larchev and S. Popova, J. Less-Common Met. **87**, 53 (1982).

[61] F. Y. Bruno, A. Tamai, Q. S. Wu, I. Cucchi, C. Barreteau, A. de la Torre, S. McKeownWalker, S. Riccò, Z. Wang, T. K. Kim, M. Hoesch, M. Shi, N. C. Plumb, E. Giannini, A. A. Soluyanov, and F. Baumberger, Phys. Rev. B **94**, 121112 (2016).

[62] H. B. Nielsen and M. Ninomiya, Phys. Lett. **105B**, 219 (1981).

[63] C. Bradley and A. Cracknell, *The Mathematical Theory of Symmetry in Solids: Representation Theory for Point Groups and Space Groups* (Oxford University, New York, 2010).

[64] S. S. Tsirkin, I. Souza, and D. Vanderbilt, Phys. Rev. B **96**, 045102 (2017).

[65] J. Gooth *et al.*, Nature (London) **547**, 324 (2017).

[66] T. Zhang, Z. Song, A. Alexandradinata, H. Weng, C. Fang, L. Lu, and Z. Fang, arXiv:1705.07244.

[67] P. Tang, Q. Zhou, and S.-C. Zhang, arXiv:1706.03817.

[68] G. Chang *et al.*, preceding Letter, Phys. Rev. Lett. **119**, 206401 (2017).